

Geometric minimization of highly symmetric potentials

A. Degee¹, I. P. Ivanov^{1,2}, V. Keus^{1,3}

¹ IFPA, Université de Liège, Allée du 6 Août 17, bâtiment B5a, 4000 Liège, Belgium

² Sobolev Institute of Mathematics, Koptyug avenue 4, 630090, Novosibirsk, Russia

³ School of Physics and Astronomy, University of Southampton, Southampton SO17 1BJ, UK

September 18, 2018

Abstract

In non-minimal Higgs mechanisms, one often needs to minimize highly symmetric Higgs potentials. Here we propose a geometric way of doing it, which, surprisingly, is often much more efficient than the usual method. By construction, it gives the global minimum for any set of free parameters of the potential, thus offering an intuitive understanding of how they affect the vacuum expectation values. For illustration, we apply this method to the S_4 and A_4 -symmetric three-Higgs-doublet models. We find that at least three recent phenomenological analyses of the A_4 -symmetric model used a local, not the global minimum. We discuss coexistence of minima of different types, and comment on the mathematical origin of geometrical CP -violation and on a new symmetry linking different minima.

1 Introduction

Finding out the nature of the electroweak symmetry breaking (EWSB) is one of the hottest topics in high-energy physics these days. The first LHC data on the Higgs-like resonance at 126 GeV show intriguing deviations from the Standard Model (SM) expectations, [1], and many believe that they hint at a non-minimal Higgs mechanism of EWSB.

In the past decades, many non-minimal Higgs sectors have been considered, [2]. Typically, these sectors involve several Higgs fields interacting via the scalar potential, which is often invariant under a group of Higgs-family transformations. Once the potential is written, one then proceeds by minimizing the potential, finding the vacuum expectation value (vev) alignment, expanding the potential near this point, and calculating phenomenologically relevant quantities.

The standard procedure for minimization of the potential is to parametrize the vev's via (possibly complex) v_i , calculate $V(v_i)$, then set all $\partial V/\partial v_i = 0$, solve these equations for v_i , and finally check that the hessian at this point is positive definite. Alternatively, one can start with the desired vacuum configuration and build the potential with a prescribed symmetry around the vacuum point.

Although this method usually works well, there are several reasons why one might not be completely satisfied with it. First, sometimes the equations cannot be solved analytically.

Second, if they are solvable, they do not always give a clear intuitive picture of how the vev alignment depends on the free parameters of the potential. Third, the potentials can support several local minima, and in order to be sure that one works with the global minimum, one must check that all other possible minima of the given potential lie above the chosen one. Unfortunately, this check is done very rarely, merely because this is a difficult task on its own.

In this paper we propose a geometric method of minimization of potentials which is free from these drawbacks. Its advantages are:

- by construction, it gives the global minimum of the potential,
- one does not need to repeat the calculations for various regions of free parameters; once the main geometrical object (the orbit space) is constructed, one gets answers for all allowed free parameters,
- even in cases when the analytic minimization is impossible, it can still give useful information e.g. number of degenerate minima, symmetry breaking properties, etc.

The main drawback of this method is that it is handy only for highly symmetric potentials, so that the number of free parameters of the potential is small. However this situation takes place in many particular realizations of non-minimal Higgs sectors, and this method should indeed be useful in practical calculations.

In this paper, we will illustrate this method with the particular versions of the three-Higgs-doublet model (3HDM), the ones with the A_4 and S_4 Higgs-family symmetry group. This models has been actively studied in the past few years [3, 4, 5, 6, 7, 8], with the idea that it might provide a natural explanation to the patterns observed in the fermion mass matrices. Minimization of the potential was conducted in these papers in the standard way, and several vev alignments were used. However, we will show below that some of them correspond in fact to a local, not a global minimum; a fact that apparently went unnoticed up to now.

The structure of the paper is as follows. In Section 2 we describe our main idea, which we formulate for convenience in the context of multi-Higgs-doublet models. We illustrate the general construction in Section 3, where we discuss in detail the S_4 and A_4 -symmetric 3HDM. In Section 4 we comment on previous publications, discuss various additional aspects of the method, and finally draw our conclusions. In Appendix, for completeness, we present the Higgs mass spectra for all global minima possible in S_4 and A_4 -symmetric 3HDM.

2 Geometric minimization of symmetric potentials

Although the method we propose is rather general and can be applied to a broad range of extended Higgs sectors and perhaps beyond, we prefer to expose it in the context of N -Higgs-doublet models (NHDM). This will allow us to keep the notation simple and, at the same time, get prepared for the particular applications in 3HDM.

2.1 Orbit space in NHDM

In the N -Higgs-doublet model we introduce N Higgs doublets ϕ_a , $a = 1, \dots, N$ with identical electroweak quantum numbers. The general renormalizable Higgs potential of NHDM is constructed from the gauge-invariant bilinear combinations $(\phi_a^\dagger \phi_b)$ [11], which describe the gauge

orbits in the Higgs space¹. The space of gauge orbits (the orbit space) can be represented as a certain algebraic manifold in the space of these bilinears. It is convenient to group them in the following N^2 real bilinears:

$$r_0 = \sqrt{\frac{N-1}{2N}} \sum_a \phi_a^\dagger \phi_a, \quad r_i = \sum_{a,b} \phi_a^\dagger \lambda_{ab}^i \phi_b, \quad i = 1, \dots, N^2 - 1. \quad (1)$$

where λ^i are the generators of $SU(N)$. The orbit space as a manifold in the euclidean space \mathbb{R}^{N^2} of these bilinears was characterized algebraically and geometrically in [9]. It lies between two forward cones defined by

$$r_0 \geq 0, \quad \frac{N-2}{2(N-1)} r_0^2 \leq \vec{r}^2 \leq r_0^2. \quad (2)$$

In addition, neutral vacua always lie on the surface of the outer cone $\vec{r}^2 = r_0^2$, while charge-breaking vacua lie strictly inside, $\vec{r}^2 < r_0^2$.

In the formalism of bilinears, the Higgs potential takes the form of a general quadratic form of r_0 and r_i :

$$V = -M_0 r_0 - M_i r_i + \frac{1}{2} \Lambda_{00} r_0^2 + \Lambda_{0i} r_0 r_i + \frac{1}{2} \Lambda_{ij} r_i r_j. \quad (3)$$

The minimization of the potential can then be cast into a geometric condition of contact of two algebraic surfaces constructed in \mathbb{R}^{N^2} : the orbit space and the equipotential surfaces defined by $V = \text{const}$, see details in [10].

In the particular case of 3HDM, the bilinears are

$$\begin{aligned} r_0 &= \frac{(\phi_1^\dagger \phi_1) + (\phi_2^\dagger \phi_2) + (\phi_3^\dagger \phi_3)}{\sqrt{3}}, \quad r_3 = \frac{(\phi_1^\dagger \phi_1) - (\phi_2^\dagger \phi_2)}{2}, \quad r_8 = \frac{(\phi_1^\dagger \phi_1) + (\phi_2^\dagger \phi_2) - 2(\phi_3^\dagger \phi_3)}{2\sqrt{3}} \\ r_1 &= \text{Re}(\phi_1^\dagger \phi_2), \quad r_4 = \text{Re}(\phi_3^\dagger \phi_1), \quad r_6 = \text{Re}(\phi_2^\dagger \phi_3), \\ r_2 &= \text{Im}(\phi_1^\dagger \phi_2), \quad r_5 = \text{Im}(\phi_3^\dagger \phi_1), \quad r_7 = \text{Im}(\phi_2^\dagger \phi_3). \end{aligned} \quad (4)$$

The orbit space in 3HDM is defined by

$$r_0 \geq 0, \quad \vec{r}^2 \leq r_0^2, \quad \sqrt{3} d_{ijk} r_i r_j r_k = \frac{3\vec{r}^2 - r_0^2}{2} r_0, \quad (5)$$

and the modulus of the vector \vec{r} is restricted as

$$\frac{1}{4} r_0^2 \leq \vec{r}^2 \leq r_0^2. \quad (6)$$

2.2 Geometric minimization: the main idea

The crucial feature of passing from fields to bilinears is that the Higgs potential is simplified; it becomes a quadratic form of these new variables. This transition was used in the two-Higgs-doublet model (2HDM) [12], and it allowed one to observe and exploit interesting geometric

¹Strictly speaking, ϕ_a are operators acting on the Higgs Fock space; however, for the purposes of this paper one can view them as doublets of complex numbers.

features of the potential both in 2HDM [13] and in multi-Higgs-doublet models [10]. Here we propose to go further in this direction, and introduce new variables in terms of which the potential becomes a *linear* function.

To this end, consider an NHDM potential with a sufficiently high symmetry so that $M_i = 0$ in (3). Absence of this term is a hallmark of so-called “frustrated symmetries” in NHDM which were discussed in [14]. The quartic part of the potential contains k different terms, k usually being rather small for a highly symmetric potential. Let us generically write the potential as

$$V = -M_0 r_0 + r_0^2 \sum_{i=0}^k \Lambda_i x_i. \quad (7)$$

Here x_i are the quartic terms divided by r_0^2 , with $x_0 = 1$ by convention, and Λ_i are coefficients in front of them.

Let us now consider the variables x_i , which can always be chosen real. Calculating them for all possible field configurations (or for all possible values of r ’s inside the orbit space) will fill a certain region in the space \mathbb{R}^k . This region, which we denote by Γ , is the orbit space “squashed” into the x_i space. Note that the map from r ’s to x_i is not, generally speaking, injective because different r ’s can correspond to the same point x_i .

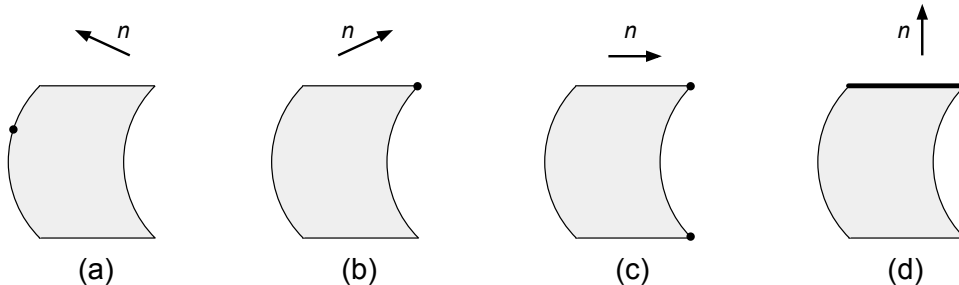


Figure 1: Two-dimensional illustration of the geometric minimization method. Shown are four cases with the same orbit space Γ (represented by the shaded region) but with different values of the parameters Λ_i , which define the direction of steepest descent \vec{n} . The four cases show how the local geometry of Γ determines the stability and degeneracy of the global minimum; (a): locally convex geometry leads to a single global minimum indicated by the dot, whose position is sensitive to the exact values of Λ_i ; (b): a minimum at a vertex is stable against variations of Λ_i ; (c): cusps separated by a concave region allow two distinct minima to coexist and be degenerate; (d): straight segments can lead to a continuum of global minima (shown by a thick line) for the special values of the parameters, implying presence of massless bosons.

Suppose the geometric shape of Γ is known. Then the minimization of the potential proceeds in three simple steps. First, since the potential (7) is a linear function of x_i , we can introduce the “direction of steepest descent” of the potential, $\vec{n} = -(\Lambda_1, \dots, \Lambda_k)$. The potential can then be written as

$$V = -M_0 r_0 + r_0^2 (\Lambda_0 - \vec{n} \cdot \vec{x}). \quad (8)$$

Then the minimum of the potential is achieved at the points of Γ which protrude farthest in the direction of \vec{n} . Once these points x_i are known, we can find their realizations in terms

of fields, and, finally, find the value of r_0 . Note that the positivity conditions require that $\Lambda_0 - \vec{n}\vec{x} > 0$ everywhere in Γ .

Some phenomenologically relevant properties of the minima follow from this geometric picture, which we illustrate in Fig. 1 with a two-dimensional example. If Γ has a smooth and strictly convex local shape, Fig. 1a, then the minimum is unique in the x_i space. It is also seen that the minimum point continuously changes if parameters Λ_i are varied. If Γ , instead, has vertices, see Fig. 1b, then the minimum point becomes stable within certain regions of Λ_i variation (or alternatively, regions of possible directions of \vec{n}). Note that such a feature is the origin of geometric CP -violation in multi-doublet models, see our discussion in Sect. 4.3. At the borders of these regions, two concurrent minima become degenerate and coexist, Fig. 1c; crossing this border causes a first order phase transition between the two vacuum configurations. Finally, if Γ contains straight segments, Fig. 1d, then for the borderline parameters Λ_i we get a continuum of global minima, which means that the model contains additional massless scalars.

In this picture, the key object becomes the shape of Γ rather than the parameters of the potential. Once the symmetry group is fixed and Γ is constructed, many properties of the potential (points of minimum, their degeneracy and coexistence, patterns of symmetry breaking, the phase diagram of the model and phase transitions) can be immediately read from its shape.

3 A_4 and S_4 -symmetric 3HDM

3.1 The potentials

In this Section we will illustrate how the general method works with the example of A_4 and S_4 -symmetric 3HDM.

The A_4 -symmetric 3HDM can be represented by the following potential

$$\begin{aligned}
V = & -\frac{M_0}{\sqrt{3}} \left(\phi_1^\dagger \phi_1 + \phi_2^\dagger \phi_2 + \phi_3^\dagger \phi_3 \right) + \frac{\Lambda_0}{3} \left(\phi_1^\dagger \phi_1 + \phi_2^\dagger \phi_2 + \phi_3^\dagger \phi_3 \right)^2 \\
& + \frac{\Lambda_3}{3} \left[(\phi_1^\dagger \phi_1)^2 + (\phi_2^\dagger \phi_2)^2 + (\phi_3^\dagger \phi_3)^2 - (\phi_1^\dagger \phi_1)(\phi_2^\dagger \phi_2) - (\phi_2^\dagger \phi_2)(\phi_3^\dagger \phi_3) - (\phi_3^\dagger \phi_3)(\phi_1^\dagger \phi_1) \right] \\
& + \Lambda_1 \left[(\text{Re} \phi_1^\dagger \phi_2)^2 + (\text{Re} \phi_2^\dagger \phi_3)^2 + (\text{Re} \phi_3^\dagger \phi_1)^2 \right] \\
& + \Lambda_2 \left[(\text{Im} \phi_1^\dagger \phi_2)^2 + (\text{Im} \phi_2^\dagger \phi_3)^2 + (\text{Im} \phi_3^\dagger \phi_1)^2 \right] \\
& + \Lambda_4 \left[(\text{Re} \phi_1^\dagger \phi_2)(\text{Im} \phi_1^\dagger \phi_2) + (\text{Re} \phi_2^\dagger \phi_3)(\text{Im} \phi_2^\dagger \phi_3) + (\text{Re} \phi_3^\dagger \phi_1)(\text{Im} \phi_3^\dagger \phi_1) \right], \tag{9}
\end{aligned}$$

or, in terms of bilinears,

$$\begin{aligned}
V = & -M_0 r_0 + \Lambda_0 r_0^2 + \Lambda_1 (r_1^2 + r_4^2 + r_6^2) + \Lambda_2 (r_2^2 + r_5^2 + r_7^2) + \Lambda_3 (r_3^2 + r_8^2) \\
& + \Lambda_4 (r_1 r_2 + r_4 r_5 + r_6 r_7). \tag{10}
\end{aligned}$$

Here parameters M_0 and Λ_i are assumed to take generic values. This potential is symmetric under the full achiral tetrahedral group T_d isomorphic to $A_4 \rtimes \mathbb{Z}_2$ of order 24. This group is generated by independent sign flips of individual doublets, by cyclic permutations of the three

doublets, as well as by a specific type of generalized- CP transformation (the CP -conjugation combined with exchange of any two doublets).

An alternative way to parametrize the potential was used in [4, 5, 7, 8]. Our coefficients are related with the coefficients of the alternative parametrization used in [7] as

$$-\frac{M_0}{\sqrt{3}} = \mu^2, \quad \Lambda_0 = 3\lambda_1 + \lambda_3, \quad \Lambda_3 = -\lambda_3, \quad \Lambda_{1,2} = \lambda_4 \pm \lambda_5 \cos \epsilon, \quad \Lambda_4 = -2\lambda_5 \sin \epsilon. \quad (11)$$

If $\Lambda_4 = 0$, we get the S_4 -symmetric 3HDM. In the alternative parametrization, this is equivalent to setting $\epsilon = 0$. The potential becomes now symmetric under the full achiral octahedral group O_h isomorphic to $S_4 \times \mathbb{Z}_2$ of order 48, which is generated by sign flips of the individual doublets, by their permutations, and by the CP -conjugation.

Since the classification of the finite realizable symmetry groups of the scalar sector in 3HDM is now known [15], we know that restricting the parameters further will never produce any larger finite symmetry group. It can only lead to continuous symmetry groups, which are necessarily frustrated and must therefore be spontaneously broken and produce massless scalars [14]. We disregard this situation on phenomenological grounds.

3.2 The orbit space in the S_4 case

Let us start with the more restricted model, the S_4 -symmetric 3HDM. Written in terms of bilinears, the potential takes form

$$\begin{aligned} V &= -M_0 r_0 + \Lambda_0 r_0^2 + \Lambda_1(r_1^2 + r_4^2 + r_6^2) + \Lambda_2(r_2^2 + r_5^2 + r_7^2) + \Lambda_3(r_3^2 + r_8^2) \\ &= -M_0 r_0 + r_0^2(\Lambda_0 + \Lambda_1 x + \Lambda_2 y + \Lambda_3 z), \end{aligned} \quad (12)$$

with the vector (x, y, z) playing the role of x_i . The positivity conditions for the potential require that

$$\Lambda_0 + \Lambda_1 x + \Lambda_2 y + \Lambda_3 z > 0 \quad (13)$$

everywhere in the orbit space. Using the properties of bilinears mentioned in Section 2, we conclude that the three-dimensional orbit space Γ must lie inside the truncated pyramid defined by

$$x, y, z \geq 0, \quad \frac{1}{4} \leq x + y + z \leq 1. \quad (14)$$

In addition, it turns out that $y \leq 3/4$. Indeed, y can be rewritten as

$$y = \frac{3}{4} \left[1 - \frac{2(\kappa_{12} + \kappa_{23} + \kappa_{31}) + Q_{\alpha\beta} Q_{\alpha\beta}^*}{(\rho_1 + \rho_2 + \rho_3)^2} \right], \quad (15)$$

where

$$\rho_a = (\phi_a^\dagger \phi_a) \geq 0, \quad \kappa_{ab} = \rho_a \rho_b - |\phi_a^\dagger \phi_b|^2 \geq 0, \quad Q_{\alpha\beta} = \sum_a \phi_a^\alpha \phi_a^\beta, \quad (16)$$

with $a = 1, 2, 3$ numbering the doublets and $\alpha, \beta = +, 0$ denoting the upper and lower components inside doublets. The largest value of y equal to $3/4$ is attained when, first, all $\kappa_{ab} = 0$ which selects the neutral vacuum, and then when the lower components of the doublets sum up as $\sum (\phi_a^0)^2 = 0$.

The exact shape of the orbit space which we found by numerical methods² is rather complicated, see Fig. 2, left. It has the form of a wedge with the edge at $x + z = 1, y = 0$ and the convex backside at small values of $x + z$. However if we focus only on the phenomenologically relevant case of neutral vacuum, then we limit ourselves only to one of its faces defined by $x + y + z = 1$. The rest of Γ corresponds to charge-breaking vacua and is disregarded.

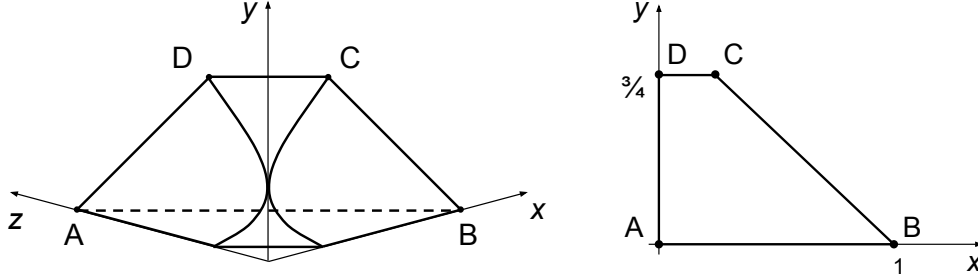


Figure 2: Left: sketch of the orbit space Γ of the S_4 -symmetric 3HDM in the (x, y, z) -space. Right: the neutral orbit space in the (x, y) -plane. On each plot, the four dots A , B , C , and D mark the positions of the possible neutral global minima.

This neutral part of the orbit space has the shape of a trapezoid, which can be established analytically using (14) and (15). We show it in Fig. 2, right, on the (x, y) -plane (with z defined as $z = 1 - x - y$). The vev alignments corresponding to the four vertices of the trapezoid are (here we give only the relative magnitude of the vev's)

$$A : (1, 0, 0), \quad B : (1, 1, 1), \quad C = (e^{i\pi/3}, e^{-i\pi/3}, \pm 1), \quad D = (e^{i\pi/4}, e^{-i\pi/4}, 0) \simeq (1, i, 0), \quad (17)$$

while the straight segments joining them are

$$\begin{aligned} AB : (v_1, v_2, v_3) \text{ with all } v_i \in \mathbb{R}, \quad BC : (e^{i\xi_1}, e^{i\xi_2}, e^{i\xi_3}), \\ AD : (v_1, iv_2, 0) \text{ with all } v_i \in \mathbb{R}, \quad CD : (e^{i\xi}, e^{-i\xi}, r) \text{ with } \cos 2\xi = -\frac{r^2}{2}. \end{aligned} \quad (18)$$

Of course, in each case we allow for arbitrary permutations of the doublets. For example, vertex D corresponds to six degenerate minima $(1, \pm i, 0), (1, 0, \pm i), (0, 1, \pm i)$.

3.3 Minimization of the S_4 -symmetric potential

Applying the methods of Section 2.2, we immediately conclude that the S_4 -symmetric 3HDM can have only four types of neutral minima without producing massless scalars, which correspond to the vertices (17). Thus, we located all possible positions of the global minimum without the need to calculate any derivatives.

It is also possible to obtain conditions on Λ_i which lead to a minimum at each of these four points just by looking at the orbit space. For example, the vev alignment of the type $(1, 0, 0)$ becomes the global minimum, when $\Lambda_3 < 0$ and $\Lambda_1, \Lambda_2 > \Lambda_3$. When these conditions are satisfied, the point A indeed lies farthest along the direction \vec{n} . In addition, the positivity condition (13) in this case implies that $\Lambda_0 + \Lambda_3 > 0$.

²We generated one million points with random up and down components of the three doublets. For each point we calculated the values of x , y , and z , and then plotted all points. By looking at the resulting 3D scatter plot from different angles, we reconstructed the shape and drew the sketch in Fig. 2.

3.4 Unexpected symmetry of the orbit space

The S_4 -symmetric 3HDM possesses a curious feature which could be noticed but would receive no explanation with the usual calculations.

First, field content of the scalar sector, after the electroweak symmetry breaking, is the following: apart from the usual three “would-be” Goldstone bosons, we have two pairs of charge-conjugate Higgses H_i^\pm , and five neutral scalars. The oscillation mode in the direction of vev’s will be denoted as h , while the other neutral Higgses are generically labeled as H_i . In (generalized) CP -conserving cases, these can be additionally classified as (generalized) CP -even and CP -odd states.

Let us now calculate the masses of the physical Higgs bosons in the two vev alignments: $(1, 1, 1)$ and $(1, 0, 0)$. In both cases we use $v^2 \equiv v_1^2 + v_2^2 + v_3^2$. The alignment $(1, 1, 1)$ becomes the global minimum of the potential if

$$\Lambda_1 < 0, \quad \Lambda_0 > |\Lambda_1| > -\Lambda_2, -\Lambda_3. \quad (19)$$

The minimum point is then parametrized as $(v, v, v)/\sqrt{6}$ with

$$\begin{aligned} v^2 &= \frac{\sqrt{3}M_0}{\Lambda_0 - |\Lambda_1|}, \\ m_{H_i^\pm}^2 &= \frac{1}{2}|\Lambda_1|v^2 = \frac{\sqrt{3}M_0}{2} \frac{|\Lambda_1|}{\Lambda_0 - |\Lambda_1|} \quad (\text{double degenerate}), \\ m_{H_i}^2 &= \frac{1}{2}(|\Lambda_1| + \Lambda_2)v^2 = \frac{\sqrt{3}M_0}{2} \frac{|\Lambda_1| + \Lambda_2}{\Lambda_0 - |\Lambda_1|} \quad (\text{double degenerate}), \\ &\quad \frac{1}{3}(|\Lambda_1| + \Lambda_3)v^2 = \frac{M_0}{\sqrt{3}} \frac{|\Lambda_1| + \Lambda_3}{\Lambda_0 - |\Lambda_1|} \quad (\text{double degenerate}), \\ m_h^2 &= \frac{2}{3}(\Lambda_0 - |\Lambda_1|)v^2 = \frac{2}{\sqrt{3}}M_0. \end{aligned} \quad (21)$$

The alignment $(1, 0, 0)$ becomes the global minimum if

$$\Lambda_3 < 0, \quad \Lambda_0 > |\Lambda_3| > -\Lambda_2, -\Lambda_1. \quad (22)$$

Expanding the potential around the point $(v, 0, 0)/\sqrt{2}$, we get

$$\begin{aligned} v^2 &= \frac{\sqrt{3}M_0}{\Lambda_0 - |\Lambda_3|}, \\ m_{H_i^\pm}^2 &= \frac{1}{2}|\Lambda_3|v^2 = \frac{\sqrt{3}M_0}{2} \frac{|\Lambda_3|}{\Lambda_0 - |\Lambda_3|} \quad (\text{double degenerate}), \\ m_{H_i}^2 &= \frac{1}{2}(|\Lambda_3| + \Lambda_2)v^2 = \frac{\sqrt{3}M_0}{2} \frac{|\Lambda_3| + \Lambda_2}{\Lambda_0 - |\Lambda_3|} \quad (\text{double degenerate}), \\ &\quad \frac{1}{2}(|\Lambda_3| + \Lambda_1)v^2 = \frac{\sqrt{3}M_0}{2} \frac{|\Lambda_3| + \Lambda_1}{\Lambda_0 - |\Lambda_3|} \quad (\text{double degenerate}), \\ m_h^2 &= \frac{2}{3}(\Lambda_0 - |\Lambda_3|)v^2 = \frac{2}{\sqrt{3}}M_0. \end{aligned} \quad (24)$$

It is hard to miss a remarkable symmetry between these mass spectra: upon exchange $\Lambda_1 \leftrightarrow \Lambda_3$ they *almost* turn into one another. The only quantity that violates this otherwise perfect symmetry is the mass of one pair of neutral Higgses.

The bizarre aspect of this almost perfect symmetry is that it is *not a symmetry of the model*. It would be a symmetry if there existed a transformation of fields that could swap x and z while keeping y unchanged. But such transformation does not exist. This is also consistent with the fact that $\Lambda_1 \leftrightarrow \Lambda_3$ does not lead to an exact matching of the two Higgs spectra.

We can trace the origin of this near symmetry from the shape of the orbit space Γ in the (x, y, z) space. Our numerical study offers very strong hints that this shape is indeed $x \leftrightarrow z$ symmetric; unfortunately, we do not have an analytic proof of this fact. Provided this is true, it explains why conditions (19) and (22) and the charged Higgs masses (which are also related with the shape of the orbit space) are exactly symmetric.

It is interesting to notice that, for both vev alignments, the spectrum of the Higgs bosons is *2HDM-like*. Namely, we have only one value for the charged Higgs masses and three values for neutral Higgs masses, just as expected for the generic 2HDM. How this situations can be distinguished from the true 2HDM experimentally, and which observable quantities one should look at, is a separate issue worth investigating further. However the origin of this 2HDM-like spectra is different in these two cases. In the vev alignment $(1, 1, 1)$ it comes from the unbroken S_3 -symmetry of the model, [3], while for the $(1, 0, 0)$ alignment, the origin is the $O(2)$ -symmetry mixing the second and third doublets, which is manifest in the vev's and the mass terms. These two symmetry arguments are non-equivalent and cannot be related to each other. After all, the two vev alignments also differ in the number of degenerate vacuum points: four for the $(1, 1, 1)$ and three for $(1, 0, 0)$.

The same relation holds between the other two possible vev alignments, see Appendix. It would be interesting to see if this approximate symmetry leads to other phenomenological similarities between these pairs of minima.

3.5 The orbit space in the A_4 case

We write the generic potential of the A_4 -symmetric 3HDM (10) in the way suggested in Sec. 2.2:

$$V = -M_0 r_0 + r_0^2 (\Lambda_0 + \Lambda_1 x + \Lambda_2 y + \Lambda_3 z + \Lambda_4 t), \quad (25)$$

with the same x, y, z as in Eq. (12) and with $t = (r_1 r_2 + r_4 r_5 + r_6 r_7) / r_0^2$.

Again, we focus on the neutral orbit space Γ , for which we choose x, y , and t as independent variables, and then $z = 1 - x - y$. The shape of Γ which arises from our numerical study is shown in Fig. 3 in the (x, y, t) space. Despite being rather complicated, it displays a remarkable triangle symmetry. Basically, it is a right circular cone oriented along the direction $x - y = t = 0$ with the apex at the origin and with opening angle $\pi/2$ and with directrix lines of length 1. Parts of this cone starting from distance $3/4$ from the apex are carved out. It has four flat faces which have the shape of deltoid (3-vertex cusped closed curve). These are located at the bottom face (defined by $z = 0$) and at three side faces (one is $y = 3/4$ and the remaining two are obtained by the $2\pi/3$ rotation of the cone). Directrix lines opposite to these three side faces have length 1 and extend up to the points B, C and C' where three flat deltoid regions meet. The remaining portions of Γ are concave regions. The two-dimensional neutral orbit space for the S_4 -symmetric model, Fig. 2, right, is simply the (x, y) -projection of

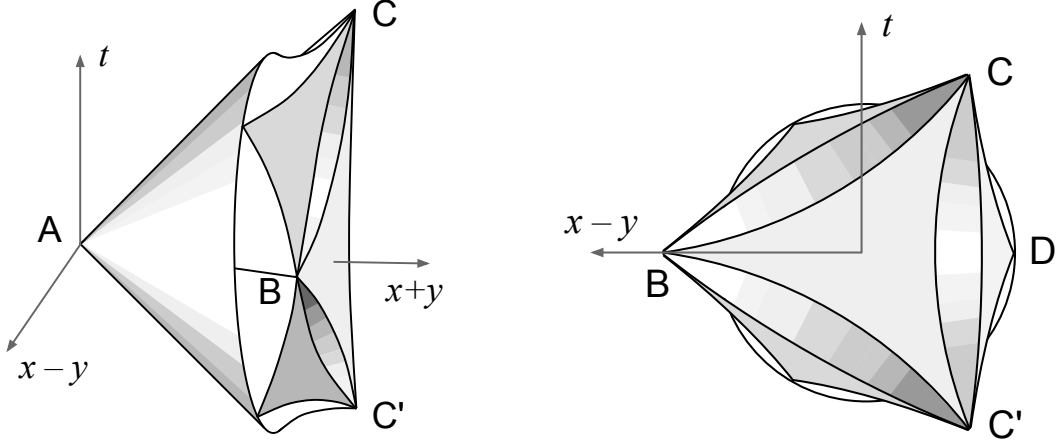


Figure 3: Sketch of the neutral orbit space in the tetrahedral 3HDM viewed from two angles. Uniformly shaded regions correspond to flat faces, graded shading indicates curved faces.

this Γ ; correspondence between the vertex points in the two shapes should be clear. We only mention that point D , which was a vertex in the S_4 case, becomes a regular point on the rim of the cone in the A_4 case.

The conical shape of the orbit space can be understood in the following way. Let us introduce two real vectors

$$\vec{a} = \frac{1}{r_0}(r_1, r_4, r_6), \quad \vec{b} = \frac{1}{r_0}(r_2, r_5, r_7), \quad (26)$$

and denote the angle between them by ξ . Then, $x = \vec{a}^2$, $y = \vec{b}^2$, $t = (\vec{a}\vec{b}) = \sqrt{xy} \cos \xi$. If it is possible for a given point (x, y) to find two parallel vectors \vec{a} and \vec{b} , then the orbit space extends in the t -direction up to $t = \sqrt{xy}$, which precisely defines the cone. It turns out that parallel vectors \vec{a} and \vec{b} exist within the triangle $0 \leq x + y \leq 3/4$ (vev alignment is $(v_1, v_2 e^{i\alpha}, 0)$), and along the straight segments defined by $y = 0$ (vev alignment (v_1, v_2, v_3)) and defined by $y/x = 3$ (alignment $(v_1 e^{i\pi/3}, v_2 e^{-i\pi/3}, v_3)$).

Let us also stress that the emergent triangle symmetry of the orbit space is *not* related to the symmetry of the potential, but is a feature of the orbit space itself. There is simply no field transformation that realizes rotations of the cone. In this aspect, this emergent symmetry is similar to the (x, z) reflection symmetry of the orbit space in the S_4 -symmetric model.

3.6 Minimization of the A_4 -symmetric potential

The shape of the orbit space immediately leads to the list of possible phenomenologically acceptable global minima (i.e. minima not leading to additional massless scalars). These are: the apex of the cone (point A), the three vertices (points B , C and C'), and the rim of the cone ($x + y = 3/4$, $t^2 = xy$). Any other point either leads to additional Goldstone bosons or is never a global minimum.

In Appendix, we analyze all these points in some detail and give the Higgs mass spectra. Comparing these spectra for different minimum points also shows intriguing relation with the triangle symmetry of the orbit space.

To our knowledge, this is the first complete solution of the minimization problem in the A_4 -symmetric 3HDM.

4 Discussion and conclusions

4.1 Comments on previous publications

The A_4 -symmetric 3HDM has received much attention, [3, 4, 5, 6, 7, 8], because spontaneous breaking of A_4 can generate interesting patterns in fermion mass matrices. In most papers, the authors just pick up a minimum with specific vev alignment, build a potential which indeed has a minimum at that point, and then proceed with analysis in the fermion sector. In particular, in [4, 5] the following vev alignment was used:

$$(e^{i\alpha}, e^{-i\alpha}, r), \quad (27)$$

with r and α being independent real parameters. Fitting the model to the fermion observables gave $r \sim 40$ in [4] and $r \sim 240$ in [5].

The authors of [7] aimed at a complete description of possible vev alignments in the minima of the A_4 -symmetric 3HDM. They critically reanalyzed the phenomenological situation arising at the minimum (27) and argued that it is strongly disfavored by the flavor physics constraints. However, they also considered this vev alignment as a viable solution of the minimization problem³.

This vev alignment is *absent* in our classification because it cannot be the global minimum. One can see it most easily precisely in the case of large r . Indeed, in our notation, this point corresponds to z being close to 1 and, therefore, it lies strictly *inside the cone* and close to its apex. This point would emerge at the surface of the cone only for angle α multiple of $\pi/3$, but in this case one would get massless scalars. This means that even if this point happens to be a minimum, it is a local, not the global one.

Thus, we prove that the phenomenological analyses of [4, 5] and, partly, of [7] correspond to a metastable electroweak vacuum. Apparently, this fact went unnoticed because the authors of these publications did not check whether the potential they got possesses a deeper minimum.

It is generally believed that the Universe sits in the global minimum of the Higgs potential, because the early hot Universe while cooling down through electroweak temperatures either selected the global minimum or, even if it were stuck in a metastable vacuum, had enough time to tunnel to the absolute minimum. Taken seriously, this argument implies that much of the analyses of [4, 5] is not phenomenologically relevant on these grounds, even without appealing to the flavor physics constraints.

4.2 Relation between the symmetry group and the vacuum structure

The two examples which we considered in full detail hint at a general relation between the symmetry group and the vacuum structure: the higher the symmetry group is, the more symmetric is the vacuum alignment. One facet of this relation is that vev alignments, which

³We are thankful to Luca Merlo who clarified to us the motivation behind the works [7, 8].

cannot be global minima for a very symmetric model, might become viable global minima if the symmetry of the potential is lowered.

Indeed, in the S_4 -symmetric 3HDM, the vev alignment $(1, e^{i\alpha}, 0)$ with generic α is buried deep in the orbit space, and it definitely cannot be the global minimum. However, in the A_4 -symmetric 3HDM, this alignment corresponds to the rim of the cone, and it becomes a viable minimum for certain non-zero Λ_4 . Geometrically, the extra term in the potential gives an additional dimension to the orbit space, and in this way it can bring the interior points of the lower-dimensional orbit space to the surface of the higher-dimensional orbit space.

Turning again to the vev alignment (27) considered in the papers [4, 5, 7], we can now speculate that even if it is buried deep in the orbit space of the A_4 -symmetric model, it might become a viable global minimum in a model with explicitly broken A_4 . In order for this to happen, however, the coefficients in front of the symmetry breaking terms must be sufficiently large. Such softly broken A_4 models were considered in [8], a follow-up of [7]. Unfortunately, the authors did not check the relative depths of different minima, so that it is not yet known when (27) becomes the global minimum.

4.3 Origin of geometric CP -violation

The possibility for spontaneous CP -violation is one of the motivations behind studying multi-Higgs-doublet models. In this context it is often proposed not only that a Higgs-family symmetry should allow for spontaneous CP -violation but also that it should stabilize the vev phases in the global minimum against variation of the free parameters. This situation is known as geometric CP violation, [16, 17, 18] and was originally found in the $\Delta(27)$ -symmetric 3HDM (though we note that the true Higgs-family symmetry group of that model is $\Delta(54)/\mathbb{Z}_3$, see discussion in [15]). The relative vev phases arising in geometric CP -violation are called calculable because their values follow from group theoretic arguments and do not depend on the exact values of the parameters of the potential⁴.

Using the method described in the present paper, we can pinpoint the mathematical origin of calculable phases in such models. They arise due to the presence of vertices in the orbit space Γ , see Fig. 1b,c,d, or to be more specific, vertices at points corresponding to non-zero relative phases. Absence of geometric CP phases would imply convexity of the orbit space, Fig. 1a. So, it is not the symmetry of the model *per se* that allows for calculable phases but the choice of coordinates x_i selected by the symmetry, in which the orbit space has vertices.

Our experience shows that the higher the finite symmetry group, the simpler is the geometric shape of the orbit space Γ , and the more vertices linked by straight segments it possesses. This explains why it is natural that geometric CP violation starts to appear only for sufficiently large finite symmetry groups.

4.4 Coexistence of different minima

A priori, it might happen that, for some values of the parameters of the potential, two (or

⁴However, we find the following statement from [17] inaccurate: “...the calculable phase arising from geometrical CP violation is uniquely determined independently of the arbitrary parameters of the scalar potential.” Indeed, parameters in any case must be such that the point realizing the geometric CP violation is the global minimum of the potential. This takes place only in a certain region but not everywhere in the space of the free parameters.

more) different types of the global minimum coexist and are degenerate. Fig. 1c illustrates this situation. Upon small variation of the parameters around this special point, one minimum point becomes the global minimum while the other turns into a local one, and it is clearly possible to make either of them the global minimum. This feature leads to a possibility of a first order phase transition upon smooth variation of the parameters, leading to important phenomenological consequences. It is therefore desirable to know, which models allow for such a possibility.

It can be inferred from Fig. 1c that this can happen if the orbit space vertices separated by a concave region, that is, if it has cusps. If instead the orbit space is a convex body, this possibility is excluded. Possibility of a first order phase transition is, therefore, linked to the non-convexity of the orbit space.

Our analysis shows that the orbit space of the S_4 -symmetric 3HDM is convex. Therefore, phenomenologically relevant global minima of different type cannot coexist in this case.

In the A_4 -symmetric 3HDM, this possibility arises. Namely, generic points on the rim of the cone and one of the three vertices B , C , or C' in Fig. 3 can be degenerate. It is also possible to make two among these three points degenerate, but not all three. Examples of such potentials can be readily constructed from geometric analysis of Fig. 3.

4.5 How general is the proposed method?

In which cases does the geometric minimization method proposed in this paper become useful? Strictly speaking, it has no intrinsic limitation. For example, in the context of the multi-Higgs-doublet models one can start with an absolutely general Higgs potential, perform a $GL(N, \mathbb{C})$ transformation in the space of doublets that brings the quadratic term to the form $M_0 r_0$ and then proceeds as discussed in Section 2.2. Of course, the potential will contain very many different terms, so that the orbit space becomes a highly non-trivial multi-dimensional shape. However comprehending it is only a human limitation, and a hypothetical computer algorithm could be able to analyze this shape looking for edges, cusps and vertices.

This method becomes much more useful when the number of distinct terms becomes small. In particular, when the dimension of the neutral orbit space is three or less, the shape can be relatively easily visualized, and one can develop a much more intuitive picture of the model than from the usual algebra. For example, in the 3HDM, this situation takes place for the following finite Higgs-family symmetry groups (based on the classification of [15]): A_4 , S_4 , $\Delta(54)/\mathbb{Z}_3$, and $\Sigma(36)$ (the last two cases not discussed in this paper). It would be interesting to see if other useful examples appear in other models.

4.6 Conclusions

In summary, we have presented a simple yet powerful and very intuitive geometric approach to minimization of highly symmetric potentials in non-minimal Higgs mechanisms. This method is capable of giving the positions of the global minima with very little calculations; in particular, it avoids the need to differentiate the potential, solve for stationary points, and check the positivity of the hessian. In a single picture, it shows all points which can be the global minimum for any values of the parameters of the potential.

For illustration purposes, we have applied this method to A_4 - and S_4 -symmetric three-Higgs-doublet models and found all points of global minimum. By doing this, we have also

proved that the vacuum point used in at least three recent phenomenological analyses of the A_4 case was not the global, but only the local minimum. We have also observed an unexpected approximate symmetry linking Higgs spectra at different minima and discussed its origin. We believe that this method can become a useful tool in all situations where minimization of highly symmetric functions is required.

Acknowledgements

It is a pleasure to acknowledge useful discussions with Pedro Ferreira, Lu s Lavoura, Rui Santos and especially with Jo o Silva, who read the draft of this paper and made numerous suggestions. I.P.I. also thanks them for hospitality at the University of Lisbon, where this paper was completed. Communications with L. Merlo, S. Morisi and E. Peinado are also acknowledged. This work was supported by the Belgian Fund F.R.S.-FNRS, and in part by grants RFBR 11-02-00242-a, RF President grant for scientific schools NSC-3802.2012.2, and the Program of Department of Physics SC RAS and SB RAS "Studies of Higgs boson and exotic particles at LHC."

A Higgs spectra of the S_4 -symmetric potential

In the case of S_4 -symmetric 3HDM we analyzed the two simple vev alignments in the main text. They were shown to be approximately related to each other by the unexpected symmetry of orbit space. The remaining two points also follow this pattern. The alignment $(1, i, 0)$ becomes the global minimum if

$$\Lambda_2 < 0, \quad |\Lambda_2| > |\Lambda_3|, \quad \Lambda_1 > \Lambda_3, \quad 4\Lambda_0 + \Lambda_3 > 3|\Lambda_2|, \quad (28)$$

and at this point we have

$$v^2 = \frac{4\sqrt{3}M_0}{4\Lambda_0 + \Lambda_3 - 3|\Lambda_2|}, \quad m_{H_i^\pm}^2 = \frac{1}{2}|\Lambda_2|v^2, \quad \frac{1}{4}(|\Lambda_2| - \Lambda_3)v^2, \quad (29)$$

and the neutral Higgs masses are

$$\begin{aligned} m_{H_i}^2 &= \frac{1}{4}(\Lambda_1 - \Lambda_3)v^2 \quad (\text{double degenerate}) \\ &\quad \frac{1}{2}(|\Lambda_2| + \Lambda_3)v^2, \quad \frac{1}{2}(|\Lambda_2| + \Lambda_1)v^2 \\ m_h^2 &= \frac{1}{6}(4\Lambda_0 + \Lambda_3 - 3|\Lambda_2|)v^2 = \frac{2}{\sqrt{3}}M_0. \end{aligned} \quad (30)$$

The alignment $(\pm 1, e^{i\pi/3}, e^{-i\pi/3})$ is the global minimum if

$$\Lambda_2 < 0, \quad |\Lambda_2| > |\Lambda_1|, \quad \Lambda_3 > \Lambda_1, \quad 4\Lambda_0 + \Lambda_1 > 3|\Lambda_2|, \quad (31)$$

and at this point we have

$$v^2 = \frac{4\sqrt{3}M_0}{4\Lambda_0 + \Lambda_1 - 3|\Lambda_2|}, \quad m_{H_i^\pm}^2 = \frac{1}{2}|\Lambda_2|v^2, \quad \frac{1}{4}(|\Lambda_2| - \Lambda_1)v^2, \quad (32)$$

with the neutral Higgs masses

$$\begin{aligned}
m_{H_i}^2 &= (a + b \pm \sqrt{a^2 + b^2}) v^2 \quad (\text{double degenerate}), \quad a = \frac{|\Lambda_2| + \Lambda_1}{4}, \quad b = \frac{\Lambda_3 - \Lambda_1}{6}, \\
m_h^2 &= \frac{4\Lambda_0 + \Lambda_1 - 3|\Lambda_2|}{6} v^2 = \frac{2}{\sqrt{3}} M_0.
\end{aligned} \tag{33}$$

Again, we observe the perfect $\Lambda_1 \leftrightarrow \Lambda_3$ symmetry in v^2 , in the minimum conditions and in the charged Higgs masses.

B Higgs spectra of the A_4 -symmetric potential

Let us write for completeness the Higgs mass spectrum at all four possible points of global minimum found in the main text.

- The vev alignment $(1, 1, 1)$ remains stable in the presence of non-zero Λ_4 if it is not too large:

$$\Lambda_4^2 < 12\Lambda_1^2, \quad \Lambda_4^2 < 2(\Lambda_3 + |\Lambda_1|)(\Lambda_2 + |\Lambda_1|). \tag{34}$$

The value of v^2 is the same as in (20), while the masses become

$$\begin{aligned}
m_{H_i^\pm}^2 &= \left(\frac{1}{2} |\Lambda_1| \pm \frac{1}{4\sqrt{3}} \Lambda_4 \right) v^2, \quad m_h^2 = \frac{2}{3} (\Lambda_0 - |\Lambda_1|) v^2, \\
m_{H_i}^2 &= \frac{v^2}{12} \left[5|\Lambda_1| + 3\Lambda_2 + 2\Lambda_3 \pm \sqrt{(|\Lambda_1| + 3\Lambda_2 - 2\Lambda_3)^2 + 12\Lambda_4^2} \right] \quad (\text{double degenerate}).
\end{aligned}$$

Note that the presence of Λ_4 splits the charged Higgs masses while it preserves the degeneracy of the neutral Higgses.

- The vev alignment $(1, 0, 0)$ is also stable if Λ_4 satisfies

$$\Lambda_4^2 < 4(\Lambda_1 + |\Lambda_3|)(\Lambda_2 + |\Lambda_3|). \tag{35}$$

The value of v^2 and the masses of the charged Higgs and the non-degenerate neutral bosons are the same as in (23), while the neutral Higgses from the second and third doublets get masses

$$m_{H_i}^2 = \frac{v^2}{4} \left[\Lambda_1 + \Lambda_2 + 2|\Lambda_3| \pm \sqrt{(\Lambda_1 - \Lambda_2)^2 + \Lambda_4^2} \right] \quad (\text{double degenerate}).$$

Note that this Higgs spectrum remains 2HDM-like as it was in the S_4 case.

- The alignment $(1, e^{i\alpha}, 0)$ for a generic α parametrizes the points around the rim of the cone. For a given value of Λ_4 , the value of α corresponding to the global minimum is fixed by the relation

$$\sin 2\alpha = -\frac{\Lambda_4}{\sqrt{(\Lambda_1 - \Lambda_2)^2 + \Lambda_4^2}}, \quad \cos 2\alpha = -\frac{\Lambda_1 - \Lambda_2}{\sqrt{(\Lambda_1 - \Lambda_2)^2 + \Lambda_4^2}}. \tag{36}$$

Geometrically, this result means that the global minimum lies on the rim in the same direction as the vector \vec{n} projected on the plane of the rim. In this case we obtain

$$v^2 = \frac{4\sqrt{3}M_0}{4\Lambda_0 + \Lambda_3 - 3\tilde{\Lambda}}, \quad (37)$$

where

$$\tilde{\Lambda} \equiv -(\Lambda_1 c_\alpha^2 + \Lambda_2 s_\alpha^2 + \Lambda_4 c_\alpha s_\alpha) = \frac{1}{2} \left[\sqrt{(\Lambda_1 - \Lambda_2)^2 + \Lambda_4^2} - (\Lambda_1 + \Lambda_2) \right] > 0, \quad (38)$$

and the mass spectrum is

$$\begin{aligned} m_{H_i^\pm}^2 &= \frac{1}{2}v^2\tilde{\Lambda}, \quad \frac{1}{4}v^2(\tilde{\Lambda} - \Lambda_3) \\ m_{H_i}^2 &= \frac{1}{4}v^2 \left[-(\Lambda_3 + \tilde{\Lambda}) + (1 \pm \cos 3\alpha) \sqrt{(\Lambda_1 - \Lambda_2)^2 + \Lambda_4^2} \right], \\ &\quad \frac{1}{2}v^2(\Lambda_1 + \Lambda_2 + 2\tilde{\Lambda}), \quad \frac{1}{2}v^2(\Lambda_3 + \tilde{\Lambda}), \\ m_h^2 &= \frac{v^2}{6}(4\Lambda_0 + \Lambda_3 - 3\tilde{\Lambda}) = \frac{2M_0}{\sqrt{3}}. \end{aligned} \quad (39)$$

Note that presence of $\cos 3\alpha$ in one pair of masses is natural and it reflects the triangle symmetry of the A_4 orbit space shown in Fig. 3. All other quantities are rotationally invariant, corresponding to the rotational symmetry of the cone.

In the limit $\Lambda_4 \rightarrow 0$, we get minimum at $\alpha \rightarrow \pi/2$, $\tilde{\Lambda} \rightarrow -\Lambda_2$, and these spectra turn into the S_4 -spectra found in Section 3.4. Note also that the three points on the rim with $\cos 3\alpha = \pm 1$ can never be “good minima” because we get mass terms with coefficients $\pm(\Lambda_3 + \tilde{\Lambda})$, which cannot be made positive simultaneously. These three points lie, in fact, on the three long directrices of the cone.

- Finally, in the case of the alignment $(\pm 1, e^{i\alpha}, e^{-i\alpha})$, with $\alpha = \pi/3$, we introduce convenient notation

$$\sin \gamma = \frac{\Lambda_4}{\sqrt{(\Lambda_1 - \Lambda_2)^2 + \Lambda_4^2}}, \quad \cos \gamma = \frac{\Lambda_1 - \Lambda_2}{\sqrt{(\Lambda_1 - \Lambda_2)^2 + \Lambda_4^2}}, \quad (40)$$

and

$$\tilde{\Lambda} = \Lambda_1 c_\alpha^2 + \Lambda_2 s_\alpha^2 + \Lambda_4 c_\alpha s_\alpha = \frac{1}{2} \left[\Lambda_1 + \Lambda_2 + \cos(2\alpha - \gamma) \sqrt{(\Lambda_1 - \Lambda_2)^2 + \Lambda_4^2} \right]. \quad (41)$$

Then, the value of v^2 is

$$v^2 = \frac{\sqrt{3}M_0}{\Lambda_0 + \tilde{\Lambda}}, \quad (42)$$

the charged Higgs masses are

$$m_{H_i^\pm}^2 = -\frac{1}{2}v^2 \left(\Lambda_2 + \frac{\sqrt{3}}{2}\Lambda_4 \right) \quad \text{and} \quad -\frac{1}{4}v^2 \left(\Lambda_1 + \Lambda_2 + \frac{2}{\sqrt{3}}\Lambda_4 \right). \quad (43)$$

The neutral Higgs spectrum contains, as usual, h with mass $m_h^2 = 2M_0/\sqrt{3}$ and two pairs of degenerate Higgses with masses

$$m_{H_i}^2 = \frac{v^2}{6} \left[\Lambda_3 + \frac{3}{2}(\Lambda_1 + \Lambda_2) - 4\tilde{\Lambda} \pm \sqrt{\left(\Lambda_3 - \frac{3}{2}(\Lambda_1 + \Lambda_2) + 2\tilde{\Lambda} \right)^2 + 3[(\Lambda_1 - \Lambda_2)^2 + \Lambda_4^2] \sin^2(2\alpha - \gamma)} \right]. \quad (44)$$

In the S_4 -symmetric case ($\Lambda_4 = 0$ and $\gamma = 0$), we recover the results of Section 3.4.

For the first three cases, the Higgs spectra were also explicitly written in [7]. We have checked that our results fully coincide with theirs. For the last case, the minimum $(\pm 1, e^{i\pi/3}, e^{-i\pi/3})$ was not explicitly written and analyzed by the authors of [7]. Instead they performed a numerical analysis of various minima of the type $(r, e^{i\alpha}, e^{-i\alpha})$, but their expressions, taken literally, become indeterminate at $r = \pm 1$ and $\alpha = \pi/3$. It is conceivable that this last point, if treated as a special case, can still be recovered from their starting expressions.

References

- [1] G. Aad *et al.* [ATLAS Collaboration], Phys. Lett. B **716**, 1 (2012); S. Chatrchyan *et al.* [CMS Collaboration], Phys. Lett. B **716**, 30 (2012).
- [2] E. Accomando *et al.*, “Workshop on CP studies and non-standard Higgs physics,” arXiv:hep-ph/0608079.
- [3] E. Ma and G. Rajasekaran, Phys. Rev. D **64**, 113012 (2001).
- [4] L. Lavoura and H. Kühböck, Eur. Phys. J. C **55**, 303 (2008);
- [5] S. Morisi and E. Peinado, Phys. Rev. D **80**, 113011 (2009).
- [6] A. C. B. Machado, J. C. Montero, and V. Pleitez, Phys. Lett. B **697**, 318 (2011).
- [7] R. de Adelhart Toorop, F. Bazzocchi, L. Merlo and A. Paris, JHEP **1103**, 035 (2011).
- [8] R. de Adelhart Toorop, F. Bazzocchi, L. Merlo and A. Paris, JHEP **1103**, 040 (2011).
- [9] I. P. Ivanov and C. C. Nishi, Phys. Rev. D **82**, 015014 (2010).
- [10] I. P. Ivanov, JHEP **1007**, 020 (2010).
- [11] J. Velhinho, R. Santos and A. Barroso, Phys. Lett. B **322**, 213 (1994).
- [12] G. Sartori and G. Valente, arXiv:hep-ph/0304026; F. Nagel, “New aspects of gauge-boson couplings and the Higgs sector”, Ph.D. thesis, University Heidelberg (2004), [<http://www.ub.uni-heidelberg.de/archiv/4803>]; M. Maniatis, A. von Manteuffel, O. Nachtmann and F. Nagel, Eur. Phys. J. C **48**, 805 (2006). I. P. Ivanov, Phys. Lett. B **632**, 360 (2006); C. C. Nishi, Phys. Rev. D **74**, 036003 (2006) [Erratum-ibid.D **76**, 119901 (2007)].

- [13] I. P. Ivanov, Phys. Rev. D **75**, 035001 (2007) [Erratum-ibid. D **76**, 039902 (2007)]; Phys. Rev. D **77**, 015017 (2008).
- [14] I. P. Ivanov and V. Keus, Phys. Lett. B **695**, 459 (2011) [arXiv:1007.5305 [hep-ph]].
- [15] I. P. Ivanov and E. Vdovin, arXiv:1206.7108 [hep-ph]; arXiv:1210.6553 [hep-ph].
- [16] G. C. Branco, J. M. Gerard and W. Grimus, Phys. Lett. B **136**, 383 (1984).
- [17] I. de Medeiros Varzielas and D. Emmanuel-Costa, Phys. Rev. D **84**, 117901 (2011); I. de Medeiros Varzielas, JHEP **1208**, 055 (2012).
- [18] M. Holthausen, M. Lindner and M. A. Schmidt, arXiv:1211.6953 [hep-ph].